RESEARCH ARTICLE

CELL BIOLOGY

NAC controls cotranslational N-terminal methionine excision in eukaryotes

Martin Gamerdinger[1]†*, Min Jia[2]†, Renate Schloemer[1], Laurenz Rabl[1], Mateusz Jaskolowski[2], Katrin M. Khakzar[1], Zeynel Ulusoy[1], Annalena Wallisch[1], Ahmad Jomaa[2]‡, Gundula Hunaeus[1], Alain Scaiola[2], Kay Diederichs[3], Nenad Ban[2]*, Elke Deuerling[1]*

N-terminal methionine excision from newly synthesized proteins, catalyzed cotranslationally by methionine aminopeptidases (METAPs), is an essential and universally conserved process that plays a key role in cell homeostasis and protein biogenesis. However, how METAPs interact with ribosomes and how their cleavage specificity is ensured is unknown. We discovered that in eukaryotes the nascent polypeptide–associated complex (NAC) controls ribosome binding of METAP1. NAC recruits METAP1 using a long, flexible tail and provides a platform for the formation of an active methionine excision complex at the ribosomal tunnel exit. This mode of interaction ensures the efficient excision of methionine from cytosolic proteins, whereas proteins targeted to the endoplasmic reticulum are spared. Our results suggest a broader mechanism for how access of protein biogenesis factors to translating ribosomes is controlled.

N-terminal methionine excision from newly synthesized proteins is a universally conserved process that ensures the stability, folding, and function of cellular proteins (*1*, *2*). Cleavage is catalyzed by specific metalloproteases called methionine aminopeptidases (METAPs), which cotranslationally process their substrates at the exit of the ribosomal tunnel (*3*–*5*). Cleavage requires the free N terminus of an elongating substrate to enter a deep methionine-binding pocket in the core of the protease, where the active site is located (*6*, *7*). To reach the active site, the second amino acid after methionine must be small and uncharged (e.g., A, C, G, P, S, T, or V) (*8*). In eukaryotes, two structurally related METAPs are expressed in the cytosol, METAP1 and METAP2, which are thought to have similar substrate specificity but different ribosome interaction mechanisms (*6*, *7*, *9*, *10*). These enzymes lack a substrate recognition interface that would allow them to distinguish between substrates from different cellular compartments. If their ribosome binding were not regulated, they would cleave methionine from any nascent substrate that has a small and uncharged amino acid at the second position, including proteins with N-terminal presequences that direct proteins to the endoplasmic reticulum (ER) (fig. S1). Instead of METAPs, these substrates require binding of the ER-targeting factor signal recognition particle (SRP) (*11*–*14*), which competes with METAPs for access to the ribosome exit site (*10*). Forced N-terminal processing of ER signal peptides by METAPs [and subsequent acetylation of the neo–N terminus by N-acetyltransferases (*15*, *16*)] inhibits translocation of proteins across the ER membrane (*17*), suggesting that binding of METAPs to ribosomes must be tightly regulated by an unknown factor in vivo. However, how eukaryotic METAPs interact with ribosomes and how their binding is spatially and temporally coordinated with other nascent chain–interacting factors at the ribosome is unknown.

NAC recruits METAP1 to translating ribosomes using a long flexible tail

We sought to identify factors that regulate access of METAPs to translating ribosomes in eukaryotes. A candidate for this function is the nascent polypeptide–associated complex (NAC), an heterodimeric complex consisting of NACα and NACβ that is bound at the tunnel exit of virtually all ribosomes in the cell (*18*–*21*). NAC consists of a central globular dimerization domain from which four long, flexible tails (N and C termini) protrude (Fig. 1A) (*22*, *23*). The globular domain and the NACβ N terminus interact with the ribosome near the tunnel exit, where NAC monitors the N termini of nascent chains for the presence of ER-targeting signals. NAC then directs these substrates into the cotranslational ER protein transport pathway by recruiting SRP to ribosomes through the UBA domain in the NACα C terminus (Fig. 1A) (*24*–*26*). Conversely, NAC could channel nascent chains without signal sequences into cytosolic protein maturation pathways, where they would first need to be processed by METAPs. Consistent with such a role, knockdown of NAC by RNA interference (RNAi) resulted in strongly reduced levels of ribosome-associated METAP1 in both *Caenorhabditis elegans* (Fig. 1B) and human cells (fig. S2A). By contrast, ribosome binding of METAP2 increased in NAC-depleted animals (Fig. 1B), suggesting a compensatory mechanism for the loss of METAP1. Moreover, methionine cleavage of a METAP model substrate (fig. S2B) was markedly impaired in NAC-depleted worms and worsened when METAP2 was additionally knocked down (Fig. 1C). Therefore, the in vivo function of METAP1 seems to rely on NAC.

To test for a possible physical interaction between NAC and METAP1 on ribosomes, we performed ribosome-binding studies in vitro using purified human NAC and METAP1. In the absence of NAC, METAP1 bound only weakly to ribosomes (Fig. 1D and fig. S2C). The addition of NAC strongly enhanced ribosome association of METAP1 (Fig. 1D and fig. S2C). By contrast, METAP2 did bind effectively to ribosomes in vitro in the absence of NAC, and the addition of NAC displaced METAP2 from ribosomes (fig. S2D). These observations suggest a direct role of NAC in stabilizing METAP1 on ribosomes, whereas METAP2 binds independently of NAC.

We then used AlphaFold (*27*) to predict the structural basis of the interaction between NAC and METAP1. The obtained model suggested an interaction of the NACβ C terminus with the N-terminal zinc-finger domain of METAP1 (Fig. 1E and fig. S3, A and B). Zinc-finger domains are widespread interaction modules that can bind DNA, RNA, or proteins (*28*). This domain is present only in eukaryotic METAP1, not in METAP2 or prokaryotic METAP1 (*29*). The enzymatic activity of human METAP1 lacking the zinc-finger domain (Δ2-70, referred to as ΔN-METAP1) was comparable to that of wild-type METAP1 in vitro, suggesting that this domain does not affect the protease active site (fig. S3C). Zinc-finger domains can be unfolded by depleting the bound zinc ions using metal complexing agents (*30*). Pretreatment of purified METAP1 with the metal chelator EDTA almost completely reversed the stabilizing effect of NAC on ribosome binding of METAP1 (fig. S3D), consistent with an interaction of NAC with the zinc-finger domain as predicted by AlphaFold.

According to the AlphaFold model, the METAP1 zinc-finger domain is bound by a conserved hydrophobic motif (^{146}VPDLV^{150}) located near the end of the NACβ C-terminal arm (Fig. 1A and fig. S3A). The molecular details of this interaction closely resemble the interaction of METAP1 with the metallochaperone ZNG1, which binds

[1]Department of Biology, Molecular Microbiology, University of Konstanz, 78457 Konstanz, Germany. [2]Department of Biology, Institute of Molecular Biology and Biophysics, ETH Zurich, 8093 Zurich, Switzerland. [3]Department of Biology, Molecular Bioinformatics, University of Konstanz, 78457 Konstanz, Germany.
*Corresponding author. Email: elke.deuerling@uni-konstanz.de (E.D.); ban@mol.biol.ethz.ch (N.B.); martin.gamerdinger@uni-konstanz.de (M.G.)
†These authors contributed equally to this work.
‡Present address: Department of Molecular Physiology and Biological Physics, University of Virginia, Charlottesville, VA 22903, USA.

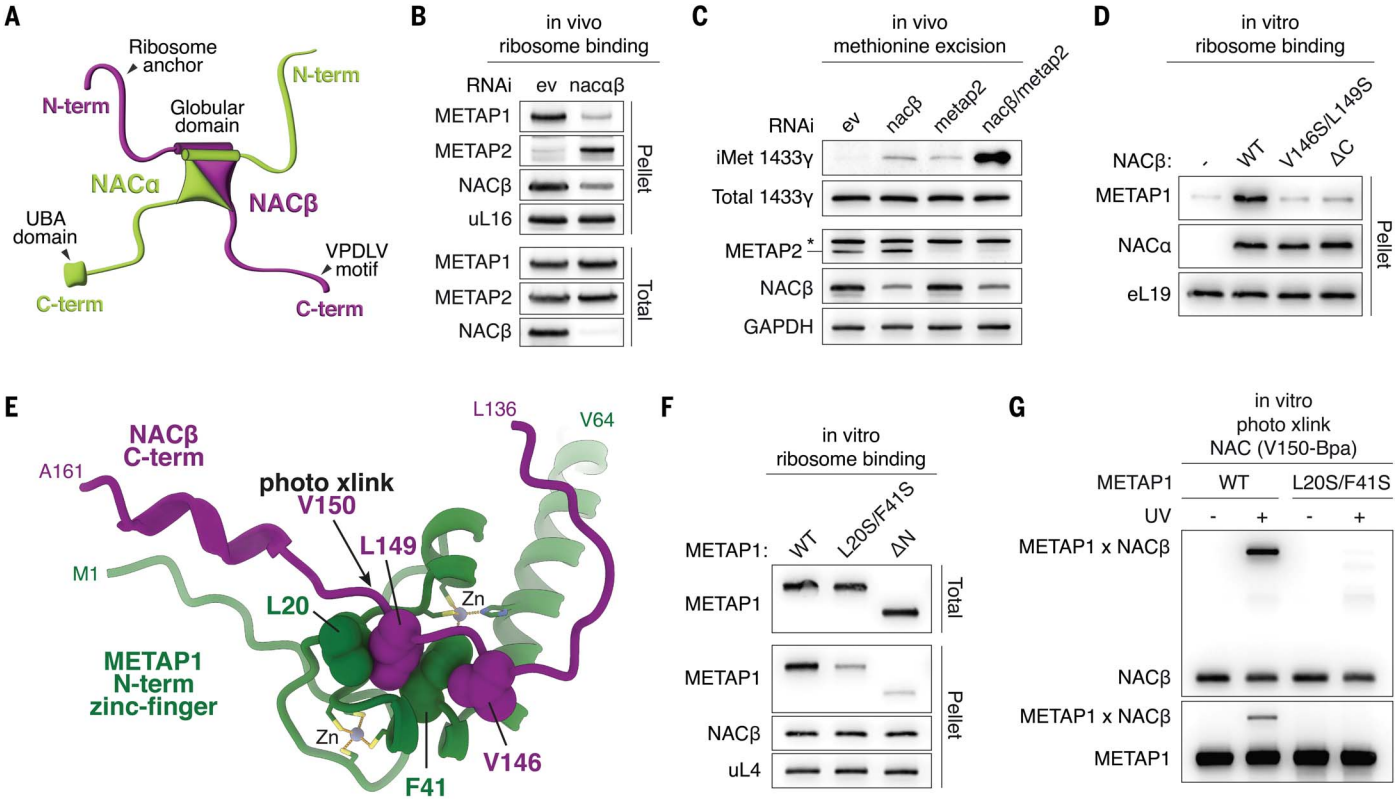

Fig. 1. A motif in the NACβ C-terminal arm binds to the zinc-finger domain of METAP1. (**A**) Model showing domain architecture of NAC consisting of a central heterodimeric globular domain and four flexible arms (N and C termini). The conserved motif (^{146}VPDLV^{150}) in the NACβ C terminus is analyzed in panels (D) to (G). (**B**) Ribosome association of METAPs after knockdown of NAC in *C. elegans*. Proteins in total and ribosomal pellet fractions were detected by immunoblotting. (**C**) Methionine cleavage of a METAP model substrate (1433γ) after knockdown of NACβ and METAP2 in *C. elegans*. Uncleaved substrate containing the initiator methionine (iMet) was detected by an epitope-specific antibody. Asterisk indicates a nonspecific band. (**D**) Ribosome binding of human METAP1 in vitro in the presence of the indicated NAC variants. (**E**) AlphaFold model of the NACβ-METAP1 interaction. The N-terminal zinc-finger domain of METAP1 (green) and the C terminus of NACβ (purple) are shown. Interacting residues are shown as spheres. Arrow marks incorporation site of a photo–cross-linking amino acid for analysis in (G). (**F**) Ribosome binding of zinc-finger mutants of METAP1 in vitro in presence of wild-type NAC. (**G**) Photo–cross-linking of NAC containing the UV-activated photo–cross-linking amino acid benzoylphenylalanine (Bpa) at position V150 indicated in (E). Photo–cross-linking was performed with wild-type METAP1 or a variant in which the two predicted NACβ-interacting residues were replaced with serine (L20S/F41S).

to the zinc-finger domain of METAP1 using a similar hydrophobic motif (*30*, *31*). To test the predicted hydrophobic interactions between the NACβ motif residues V146 and L149 and the residues L20 and F41 in the METAP1 zinc finger (Fig. 1E and fig. S4), we replaced these residues with serines (NACβ V146S/L149S and METAP1 L20S/F41S). Additionally, we investigated deletion mutants lacking the C terminus of NACβ (Δ140-162, referred to as ΔC-NACβ) or the N terminus of METAP1 (ΔN-METAP1). All mutations almost completely abolished the stabilizing effect of NAC on ribosome binding of METAP1 in vitro (Fig. 1, D and F). Moreover, a NAC variant carrying a photo–cross-linking probe at position V150 of NACβ directly adjacent to the predicted METAP1-interacting residues (Fig. 1E and fig. S3B) cross-linked strongly with wild-type METAP1, but not with the L20S/F41S mutant (Fig. 1G). Thus, NAC interacts with the METAP1 zinc-finger domain through a conserved hydrophobic motif in the long, flexible C-terminal arm of NACβ.

The binding affinity of the NACβ C-terminal tail to the METAP1 zinc-finger domain was high (K_D = 0.16 μM ± 0.02) and comparable to that of ZNG1, which shares a similar interaction motif (fig. S3, E and F) (*30*). This suggests that the NACβ C terminus provides key binding affinity for METAP1 on ribosomes. We therefore tested the importance of this interaction for N-terminal methionine excision in vivo. Consistent with the in vitro studies, ribosome binding of METAP1 was strongly reduced in *C. elegans* worms expressing the ΔC-NACβ variant, although like wild-type NAC, this NAC mutant efficiently bound to ribosomes (Fig. 2A). Ribosome association of METAP1 was also strongly decreased in human cells expressing the V146S/L149S or ΔC-NACβ mutant variants (fig. S3, G and H). Thus, the interaction of the NACβ C terminus with the METAP1 zinc-finger domain facilitates ribosome binding of METAP1 in vivo. In agreement, the METAP1 mutant lacking the N-terminal zinc-finger domain (ΔN-METAP1) was almost undetectable in the ribosomal pellet fraction of worms (Fig. 2B). Worms expressing mutant ΔC-NACβ or ΔN-METAP1 also showed a strong methionine excision defect in the METAP2 RNAi background (Fig. 2, C and D). Moreover, the viability of animals expressing the mutant NAC or METAP1 variants was severely reduced compared with wild-type animals when METAP2 expression was suppressed (Fig. 2, E and F). Thus, tethering of METAP1 to translating ribosomes through the flexible C-terminal NACβ arm is critical for methionine excision in vivo.

Mechanism of ribosome-nascent chain engagement by METAP1

The C terminus of NACβ and the N terminus of METAP1 are both flexibly tethered to the central domains of the proteins (*6*, *26*, *30*).

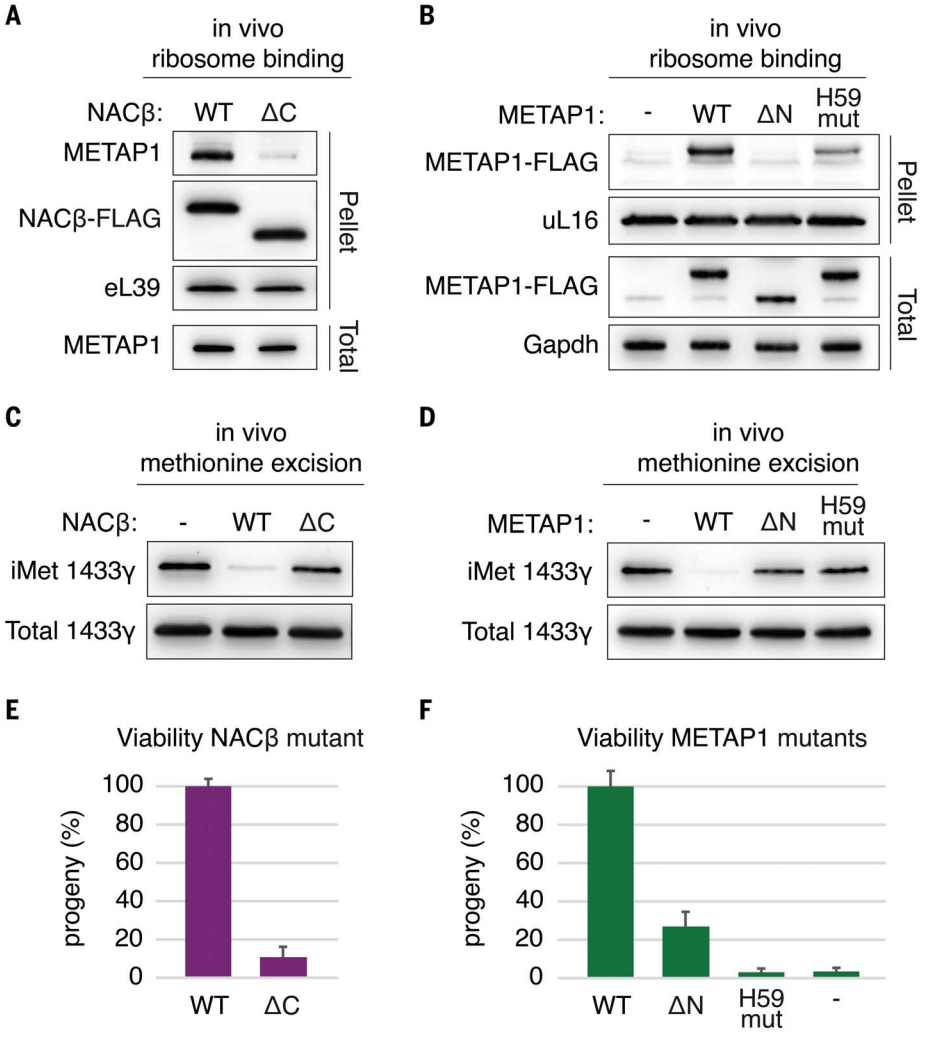

Fig. 2. NAC recruits METAP1 to ribosomes for methionine cleavage in vivo. (**A**) Ribosome association of endogenous METAP1 in *C. elegans* worms expressing the indicated FLAG-tagged NACβ variants. Proteins in the total and ribosomal pellet fractions were detected by immunoblotting. (**B**) Ribosome association of FLAG-tagged METAP1 variants with indicated mutations in *C. elegans*. METAP1 levels in the total and ribosomal pellet fractions were analyzed by immunoblotting. (**C** and **D**) Methionine cleavage of a METAP model substrate (1433γ) in worms as in (A) and (B), respectively, after knockdown of METAP2. Uncleaved substrate (iMet) was detected with an epitope-specific antibody. (**E** and **F**) Viability or worms as in (A) and (B), respectively, after knockdown of METAP2. Graph shows the number of progeny in each mutant strain relative to worms expressing wild-type NACβ or METAP1 (set to 100%). Data are shown as means ± SD (*N* = 3).

Therefore, an interaction between these flexible arms only ensures high local concentration of METAP1 in the vicinity of the ribosomal tunnel exit. However, because METAP1 did bind weakly to ribosomes in vitro in the absence of NAC (fig. S2C), some direct interactions between METAP1 and the ribosome may exist. Moreover, the ΔC-NACβ variant still showed a weak stabilizing effect on METAP1 ribosome binding (Fig. 1D and fig. S5A), suggesting a secondary contact between NAC and METAP1.

To understand how METAP1 is positioned on ribosomes to engage its substrates, we purified ribosome nascent chain complexes (RNCs) carrying a cytosolic nascent METAP substrate (GPI; 65 amino acids) and determined its structure in complex with wild-type NAC and a metal-binding deficient METAP1 variant with low catalytic activity (D220N; fig. S6) (*32*) by single-particle cryo–electron microscopy (cryo-EM). The reconstruction showed the ribosome with a peptidyl-transfer RNA, the GPI nascent chain within the ribosomal tunnel, and both NAC and METAP1 bound at the tunnel exit (Fig. 3, A to C, and figs. S7 to S9). The globular domain of NAC was found near the exit of the ribosomal tunnel as in previous structures (*26*), including the N terminus of NACβ anchored between eL22 and eL19 (Fig. 3B). The catalytic domain of METAP1 was found to interact with both the ribosome and the globular domain of NAC, orienting the methionine-binding pocket toward the exit of the ribosomal tunnel (Fig. 3C). The distance between the active site of the enzyme and the exit of the ribosomal tunnel is consistent with the cotranslational processing of nascent chains when they reach a length of ~50 amino acids (Fig. 3C and fig. S9). The N-terminal zinc-finger domain of METAP1 and the C-terminal arm of NACβ were not resolved, suggesting high flexibility even in the ribosome-bound ternary complex (Fig. 3B).

In the cryo-EM reconstruction, the globular domain of NAC was seen in contact with the central METAP1 domain in a region where a ribosome-anchoring domain is found in METAP2-related proteins (Fig. 4A and fig. S10). This explains why the globular domain of NAC displaced METAP2 but not METAP1 from ribosomes (fig. S2D). The interaction with the NAC globular domain could also explain why NAC stabilized METAP1 binding even when it was missing the C-terminal tail, as in the ΔC-NACβ mutant (fig. S5A). To investigate this, we performed in vitro binding studies with ΔC-NACβ together with two METAP1 mutants designed to disrupt the interaction with the globular domain of NAC: ^{77}PWAGY/AAAAA^{81} and ^{340}WPD/AAA^{342} (Figs. 3D and 4A). As expected, these mutants were no longer stabilized on ribosomes in the context of ΔC-NACβ (Fig. 3E). However, no substantial difference in binding was detected in the presence of wild-type NAC, indicating that the C-terminal contact of NACβ with the METAP1 zinc finger is the key contributor to the binding affinity (fig. S5B).

The cryo-EM structure also revealed a direct ribosomal contact of METAP1 involving the ribosomal protein uL23 and the ribosomal RNA (rRNA) helix H59, a known docking site for several nascent chain–associated factors (Figs. 3, B and D, and 4, B and C) (*9*, *14*, *33*, *34*). To investigate the importance of these interactions, we mutated METAP1 residues that contact uL23 (^{317}VMK/AAA^{319} and ^{127}QIK/AAA^{129}) and H59 (^{289}RS/AA^{290} + ^{308}HY/AA^{309}, referred to as H59mut; fig. S3C). The mutated clusters of residues are conserved and located in loop regions of METAP1 (Fig. 4, B and C). In the absence of NAC, the binding of these mutants to ribosomes in vitro was strongly reduced (Fig. 3F). Addition of NAC restored ribosome binding of the uL23-binding mutants almost to wild-type levels, whereas binding of the H59mut variant was still substantially reduced (fig. S5B).

These data suggest that H59 is the most important ribosome contact of METAP1 and that perturbing it would negatively affect METAP1 function. Therefore, we introduced this mutation in *C. elegans* METAP1 for in vivo analysis.

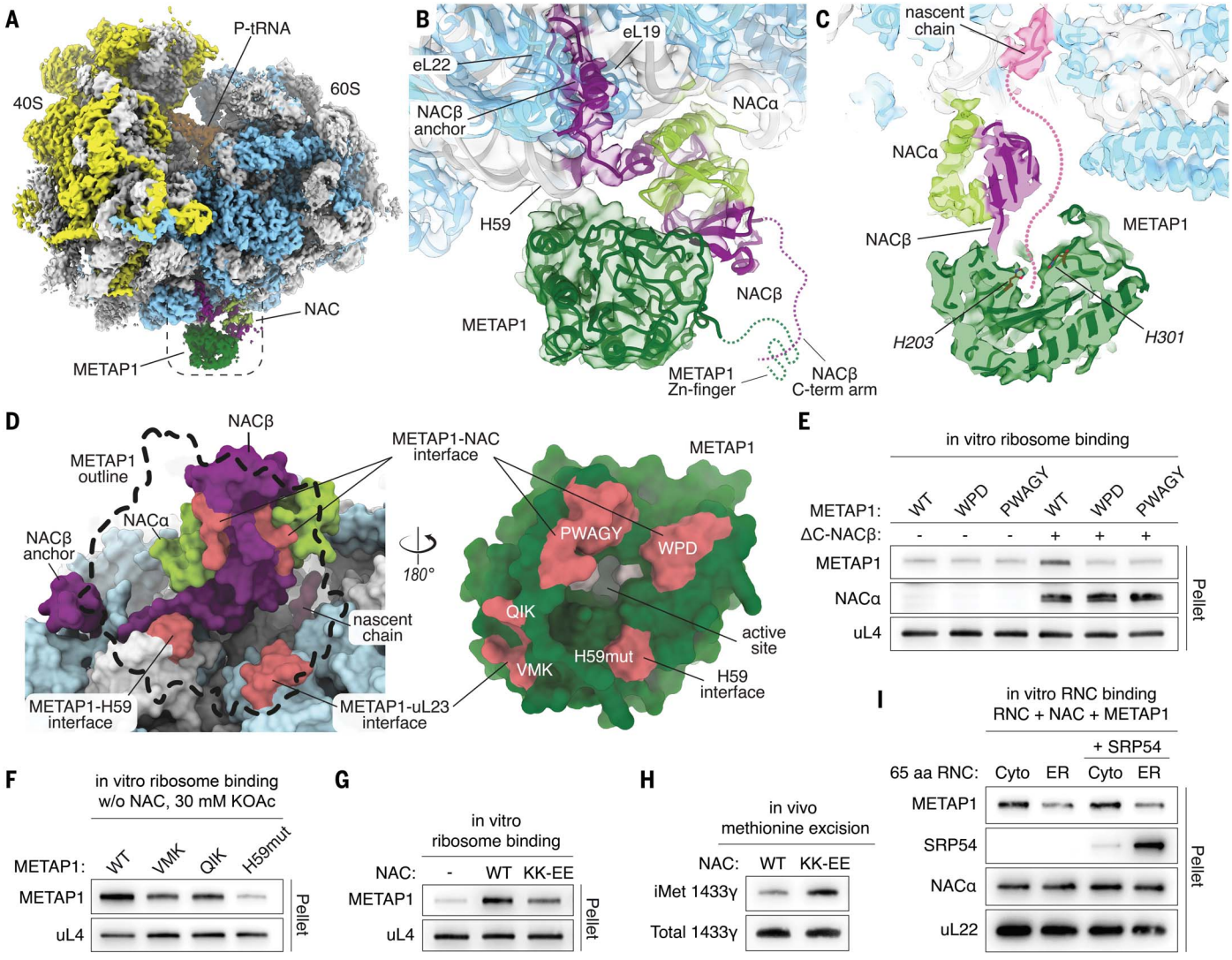

Fig. 3. Mechanism of ribosome-nascent chain engagement by METAP1. (**A**) Cryo-EM structure of the RNC-NAC-METAP1 complex. 40*S* and 60*S* proteins are colored in yellow and light blue, respectively; rRNA is shown in gray. Dashed box indicates the magnified region shown in (B). (**B**) Close-up view of the ribosomal tunnel exit. NACα is colored in yellow green, NACβ in purple, and METAP1 in dark green. Dashed lines show where the flexible NACβ C-terminal arm and the METAP1 zinc finger would protrude. (**C**) Cross section of map visualizing the METAP1 catalytic center. Dashed line indicates a potential path of a nascent chain 50 amino acids in length. Residues critical for catalytic activity (H203 and H301) are shown as sticks. (**D**) Surface representation showing METAP1-ribosome and METAP1-NAC interfaces (red). Left: interfaces on the ribosome and NAC. Dashed outline indicates position of METAP1. Right: interfaces on METAP1. (**E**) Ribosome binding of METAP1 variants carrying alanine mutations in the binding interfaces indicated in (D) in the presence of NAC lacking the NACβ C terminus (ΔC-NACβ). (**F**) Ribosome binding of METAP1 variants in vitro in the absence of NAC at low salt concentration (30 mM KOAc). Residues indicated in (D) that interact with uL23 or H59 were replaced with alanines. (**G**) Ribosome binding of METAP1 in the presence of the indicated NAC variants. KK-EE refers to a charge-reversal NAC mutant deficient in binding its globular domain to the ribosome. (**H**) Methionine cleavage of a METAP model substrate (1433γ) in *C. elegans* expressing NAC variants as in (G) after knockdown of METAP2. Uncleaved substrate (iMet) was detected by an epitope-specific antibody. (**I**) Ribosome binding of METAP1 to NAC-bound RNCs translating either a cytosolic (GPI) or an ER (HSPA5) substrate. SRP54 was used as a marker for the ER signal sequence.

Consistent with the in vitro results, disruption of the H59 contact resulted in decreased ribosome binding of METAP1 in vivo (Fig. 2B). Moreover, similar to ΔN-METAP1–expressing worms, methionine cleavage of a model substrate was strongly reduced (Fig. 2D). Additional depletion of METAP2 in animals expressing the H59 mutant also strongly impaired viability of worms (Fig. 2F). These data suggest that the ribosomal contact of METAP1 to H59 is crucial for methionine excision by ensuring the proper positioning of the enzymatic active site in front of the tunnel exit to capture the N terminus of a nascent chain (Fig. 3C).

ER signal sequences prevent docking of METAP1 to NAC-bound ribosomes

Our data show that the function of METAP1 depends on the formation of a ternary complex with NAC at the exit of the ribosomal tunnel. In the complex, NAC is positioned on the ribosome with its globular domain bound in the vicinity of the ribosomal tunnel exit (Fig. 3, A to D). In this conformation, NAC prevents the binding of the ER-targeting factor SRP (*26*). However, a nascent chain with an N-terminal ER-targeting signal sequence destabilizes the globular domain of NAC to enable SRP binding (*26*). Therefore, considering that the conformation of NAC will depend on the nature of the synthesized nascent chains, NAC will allow functional docking of METAP1 only for sequences that are lacking an ER-targeting

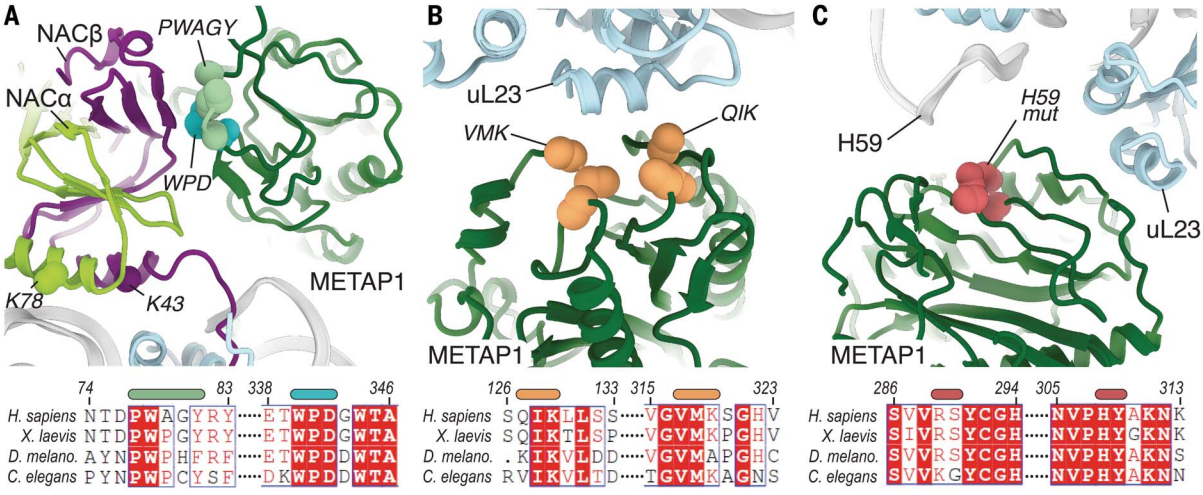

Fig. 4. METAP1 interactions with the ribosome and the NAC globular domain. (**A**) Close-up view of the binding region between METAP1 and the NAC globular domain. METAP1 residues shown as spheres were mutated to alanines in the analysis shown in Fig. 3E. Sequence alignment below shows their conservation. The indicated NAC residues K78 and K43 in the ribosome-binding helices were mutated to glutamic acid in the KK-EE NAC variant shown in Fig. 3, G and H. (**B**) Close-up view of the uL23-METAP1 interface. The residues shown as spheres that contact a short helix of uL23 were mutated to alanines in Fig. 3F. Conservation of residues is shown below. (**C**) Close-up view of the METAP1 interaction with rRNA helix H59. METAP1 residues shown as red spheres were mutated to alanines (H59mut) in the analyses shown in Figs. 2 and 3F. Sequence alignment below shows their conservation.

signal when the NAC globular domain is tightly bound at the exit of the ribosomal tunnel.

To investigate whether ribosome binding of the NAC globular domain is critical for METAP1 function, we used a previously established NAC variant with two charge reversal mutations in the positively charged helices that attach the globular domain to the tunnel exit: NACα K78E and NACβ K43E, referred to here as KK-EE NAC (Fig. 4A) (*26*). This NAC variant still binds to ribosomes through the high-affinity N-terminal NACβ anchor, whereas binding of the globular domain is weakened (*26*). We found that recruitment of METAP1 to ribosomes by KK-EE NAC was strongly reduced in vitro (Fig. 3G), and worms expressing this variant showed a marked methionine excision defect in vivo (Fig. 3H). Thus, methionine cleavage by METAP1 requires that the globular domain of NAC is bound to the tunnel exit of the ribosome. This suggests that ER-targeting signals that destabilize the globular domain of NAC also destabilize METAP1 binding. To investigate this, we used RNCs carrying a nascent chain (65 amino acids) of the ER substrate HSPA5, which contains an N-terminal signal sequence (*26*). Binding of METAP1 to NAC-bound HSPA5-RNCs was strongly reduced compared with RNCs translating a cytosolic protein (GPI; 65 amino acids) (Fig. 3I), suggesting that ER signal peptides prevent a functional docking of METAP1 to the ribosome exit site. Consistent with this, fusion of an ER signal peptide to a cytosolic nascent substrate effectively prevents methionine excision in a cell-free in vitro translation system (fig. S5C). These data are consistent with the idea that ER-targeting signals disrupt the METAP1-binding platform at the tunnel exit by destabilizing the NAC globular domain. Therefore, the conformational change in NAC triggered by ER-targeting signals restricts METAP1 binding and at the same time promotes SRP binding, whereas the effect is exactly the opposite when no ER signal sequence is present. These observations show that although METAP1 cannot distinguish between ER and cytosolic nascent substrates on its own, the high specificity for cytosolic nascent chains is cotranslationally mediated by NAC.

Discussion

On the basis of our findings, we propose a mechanistic model for how eukaryotic METAP1 can specifically engage nascent substrates for methionine excision (Fig. 5). As observed here and in a previous study (*26*), the highly abundant NAC binds to virtually all translating ribosomes in the cytosol through its NACβ anchor domain. The NAC globular domain is positioned next to the tunnel exit, where it can sense the sequence of the nascent chain emerging from the ribosomal tunnel. In the presence of an ER-targeting signal, the globular domain of NAC dissociates and allows SRP binding, whereas in the absence of an ER-targeting signal, the globular domain remains bound. METAP1 is likely directed to the ribosome-NAC complex through high-affinity interactions between the long, flexible C-terminal arm of NACβ and the N-terminal zinc-finger domain of METAP1. Our data show that formation of the productive complex, in which the catalytic pocket of METAP1 is optimally oriented toward the exit of the ribosomal tunnel to cleave methionine, requires simultaneous docking of METAP1 and the NAC globular domain to the ribosome. This mechanism explains why the N termini of ER-targeting presequences, of which nearly 50% would be susceptible to methionine excision in humans (fig. S1), are not modified in vivo (*17*), because they disrupt the composite binding platform for METAP1 on the ribosome by detaching the NAC globular domain. Therefore, signal sequences that destabilize NAC will simultaneously prevent METAP1 binding while allowing SRP to access the nascent chain at the ribosomal tunnel exit. SRP recruitment then occurs through the UBA domain at the end of the long, flexible C-terminal arm of NACα to initiate ER protein targeting (*26*). This mechanism is likely to be broadly conserved in eukaryotes, with possible additional roles of rRNA expansion segments in yeast, where NAC is not essential (*10*, *35*–*37*).

These findings show that NAC functions as a molecular control hub at the ribosomal exit site, ensuring efficient and specific binding of METAP1 and SRP to their respective nascent polypeptides emerging from the ribosomal tunnel. With its two flexible C-terminal tails, NAC ensures that the nascent chain–interacting factors are present in the vicinity of the ribosomal tunnel, whereas its globular domain controls the handover of the nascent polypeptide to the designated factor in a sequence-specific manner. This mechanism improves the specificity of N-terminal methionine excision and the fidelity of ER protein transport, both essential cellular processes. Our study further demonstrates that methionine excision in eukaryotes includes METAP2 as a redundant backup system that acts independently of NAC. How METAP2 gains regulated access to the

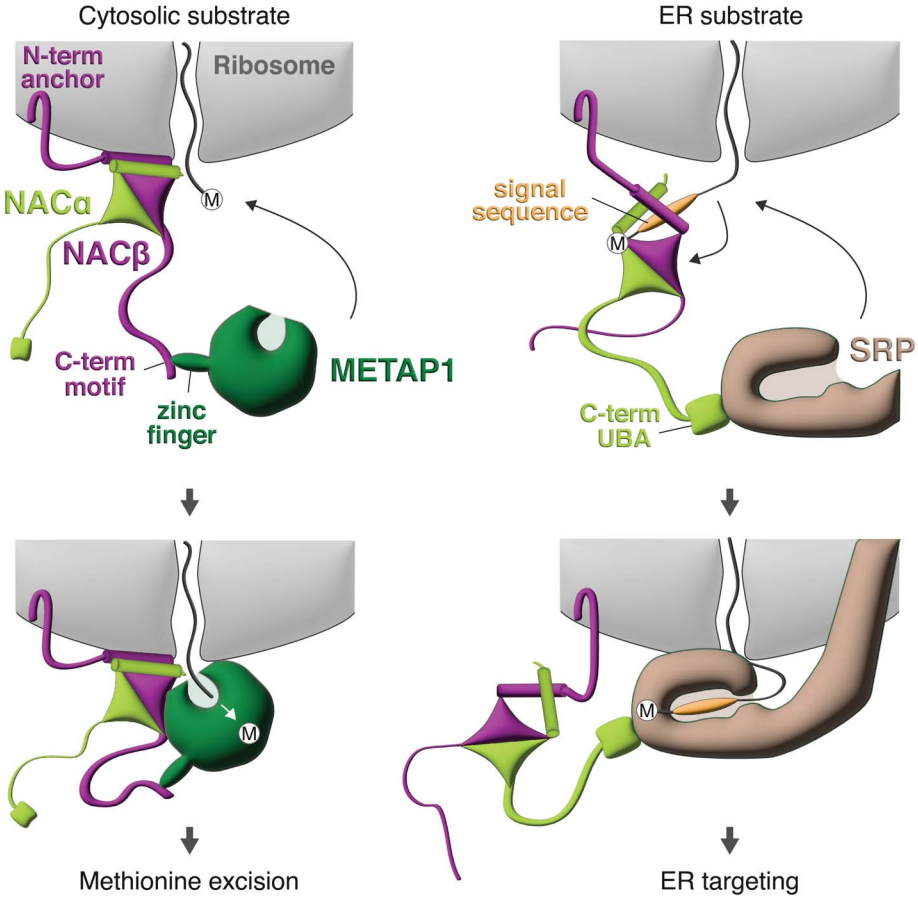

Fig. 5. Model of selective factor recruitment by NAC. NAC binds all ribosomes through the N-terminal NACβ anchor domain. On cytosolic RNCs, the NAC globular domain is attached to the ribosomal tunnel exit and forms a binding platform for METAP1 while blocking SRP binding. The local concentration of METAP1 near the exit of the ribosomal tunnel is increased through tight but flexible binding between a hydrophobic motif in the C-terminal arm of NACβ and the zinc-finger domain of METAP1 (left). An emerging ER signal sequence disrupts the METAP1-binding platform by detaching the NAC globular domain from the exit site. This also releases the SRP-binding site at the tunnel exit, leading to specific recruitment of SRP through the C-terminal arm of NACα and its UBA domain (right).

ribosome exit site in the presence of NAC is unclear. In addition to SRP and METAPs, a variety of other nascent chain–processing factors require regulated access to the ribosome exit site, including N-terminal modifying enzymes (*38*–*40*), chaperones (*41*, *42*), transport factors (*43*–*45*) and quality control factors (*46*, *47*). Understanding the potential interplay of these factors with NAC appears to be the key to understanding the mechanisms and the regulation of cotranslational protein biogenesis in human cells.

REFERENCES AND NOTES

1. R. A. Bradshaw, W. W. Brickey, K. W. Walker, *Trends Biochem. Sci.* **23**, 263–267 (1998).
2. C. Giglione, A. Boularot, T. Meinnel, *Cell. Mol. Life Sci.* **61**, 1455–1474 (2004).
3. C. Giglione, S. Fieulaine, T. Meinnel, *Biochimie* **114**, 134–146 (2015).
4. G. Kramer, D. Boehringer, N. Ban, B. Bukau, *Nat. Struct. Mol. Biol.* **16**, 589–597 (2009).
5. C. I. Yang, H. H. Hsieh, S. O. Shan, *Proc. Natl. Acad. Sci. U.S.A.* **116**, 23050–23060 (2019).
6. A. Addlagatta, X. Hu, J. O. Liu, B. W. Matthews, *Biochemistry* **44**, 14741–14749 (2005).
7. S. Liu, J. Widom, C. W. Kemp, C. M. Crews, J. Clardy, *Science* **282**, 1324–1327 (1998).
8. Q. Xiao, F. Zhang, B. A. Nacev, J. O. Liu, D. Pei, *Biochemistry* **49**, 5588–5599 (2010).
9. K. Wild *et al.*, *Nat. Commun.* **11**, 776 (2020).
10. Y. Nyathi, M. R. Pool, *J. Cell Biol.* **210**, 287–301 (2015).
11. R. Gilmore, G. Blobel, P. Walter, *J. Cell Biol.* **95**, 463–469 (1982).
12. M. Halic *et al.*, *Nature* **444**, 507–511 (2006).
13. R. M. Voorhees, R. S. Hegde, *eLife* **4**, e07975 (2015).
14. A. Jomaa *et al.*, *Cell Rep.* **36**, 109350 (2021).
15. K. K. Starheim, K. Gevaert, T. Arnesen, *Trends Biochem. Sci.* **37**, 152–161 (2012).
16. S. Deng, R. Marmorstein, *Trends Biochem. Sci.* **46**, 15–27 (2021).
17. G. M. Forte, M. R. Pool, C. J. Stirling, *PLOS Biol.* **9**, e1001073 (2011).
18. M. del Alamo *et al.*, *PLOS Biol.* **9**, e1001100 (2011).
19. M. Gamerdinger *et al.*, *Mol. Cell* **75**, 996–1006.e8 (2019).
20. B. Wiedmann, H. Sakai, T. A. Davis, M. Wiedmann, *Nature* **370**, 434–440 (1994).
21. U. Raue, S. Oellerer, S. Rospert, *J. Biol. Chem.* **282**, 7809–7816 (2007).
22. Y. Liu, Y. Hu, X. Li, L. Niu, M. Teng, *Biochemistry* **49**, 2890–2896 (2010).
23. L. Wang *et al.*, *Protein Cell* **1**, 406–416 (2010).
24. M. Gamerdinger, M. A. Hanebuth, T. Frickey, E. Deuerling, *Science* **348**, 201–207 (2015).
25. H. H. Hsieh, J. H. Lee, S. Chandrasekar, S. O. Shan, *Nat. Commun.* **11**, 5840 (2020).
26. A. Jomaa *et al.*, *Science* **375**, 839–844 (2022).
27. J. Jumper *et al.*, *Nature* **596**, 583–589 (2021).
28. S. S. Krishna, I. Majumdar, N. V. Grishin, *Nucleic Acids Res.* **31**, 532–550 (2003).
29. S. M. Arfin *et al.*, *Proc. Natl. Acad. Sci. U.S.A.* **92**, 7714–7718 (1995).
30. A. Weiss *et al.*, *Cell* **185**, 2148–2163.e27 (2022).
31. M. Pasquini *et al.*, *Cell Rep.* **39**, 110834 (2022).
32. S. Mitra, K. M. Job, L. Meng, B. Bennett, R. C. Holz, *FEBS J.* **275**, 6248–6259 (2008).
33. A. Jomaa *et al.*, *Nat. Commun.* **8**, 15470 (2017).
34. L. Kater *et al.*, *EMBO Rep.* **20**, e48191 (2019).
35. K. Fujii, T. T. Susanto, S. Saurabh, M. Barna, *Mol. Cell* **72**, 1013–1020.e6 (2018).
36. J. A. Vetro, Y. H. Chang, *J. Cell. Biochem.* **85**, 678–688 (2002).
37. S. Zuo, Q. Guo, C. Ling, Y. H. Chang, *Mol. Gen. Genet.* **246**, 247–253 (1995).
38. U. A. Friedrich *et al.*, *Cell Rep.* **34**, 108711 (2021).
39. A. G. Knorr *et al.*, *Nat. Struct. Mol. Biol.* **26**, 35–39 (2019).
40. S. Varland, C. Osberg, T. Arnesen, *Proteomics* **15**, 2385–2401 (2015).
41. Y. Chen, B. Tsai, N. Li, N. Gao, *Nat. Commun.* **13**, 3410 (2022).
42. Y. Zhang *et al.*, *Nat. Commun.* **11**, 1504 (2020).
43. S. Pfeffer *et al.*, *Nat. Commun.* **6**, 8403 (2015).
44. L. Smalinskaitė, M. K. Kim, A. J. O. Lewis, R. J. Keenan, R. S. Hegde, *Nature* **611**, 161–166 (2022).
45. R. M. Voorhees, I. S. Fernández, S. H. Scheres, R. S. Hegde, *Cell* **157**, 1632–1643 (2014).
46. S. Shao, A. Brown, B. Santhanam, R. S. Hegde, *Mol. Cell* **57**, 433–444 (2015).
47. P. S. Shen *et al.*, *Science* **347**, 75–78 (2015).

ACKNOWLEDGMENTS

We thank all laboratory members for discussions, especially M. Leibundgut for the help with interpretations of electron microscopy maps, T. Schoenhut for expressing METAP1 mutants for binding studies, and M. Kovermann and Y. Werle for help with the spectrofluorometer. **Funding:** This work was supported by the German Science Foundation (grants SFB969/A01 and A07 to E.D. and M.G.), the Swiss National Science Foundation (SNSF grant 310030_212308 to N.B.), the National Center of Excellence in Research RNA & Disease Program of the SNSF (grant 51NF40-205601 to N.B.), and the European Research Council (Synergy Grant 101072047 CoTransComplex to N.B.). **Author contributions:** M.G., M.Ji., N.B., and E.D. conceived the project. M.G. and R.S. performed in vitro biochemical analyses with help from Z.U. and A.W. M.G. and L.R. performed *C. elegans* in vivo experiments. K.K. purified RNCs and performed RNC binding studies. G.H. performed human cell-based studies. M.Ji. prepared the cryo-EM samples and collected the data with help of A.J. and A.S. M.Ja. and M.Ji. processed the cryo-EM data and created the structural figures. M.Ja. adjusted and refined the molecular model. K.D. helped to interpret the structural data. M.G., M.Ji., N.B., and E.D. wrote the manuscript. All authors contributed to data analysis and editing the final version of the manuscript. **Competing interests:** The authors declare no competing interests. **Data and materials availability:** Cryo-EM maps and model coordinates have been deposited in the Electron Microscopy Data Bank (EMDB) and Protein Data Bank (PDB) under accession codes EMD-17367 and PDB ID 8P2K, respectively.

SUPPLEMENTARY MATERIALS

science.org/doi/10.1126/science.adg3297
Materials and Methods
Figs. S1 to S10
Tables S1 to S3
References (*48*–*64*)
MDAR Reproducibility Checklist

View/request a protocol for this paper from *Bio-protocol*.

Submitted 16 December 2022; resubmitted 11 April 2023
Accepted 18 May 2023
10.1126/science.adg3297